Influence of Surface Topography on Alkanethiol SAMs Assembled from Solution and by Microcontact Printing

ARTICLE *in* LANGMUIR · APRIL 2001

Impact Factor: 4.46 · DOI: 10.1021/la001462t

3 AUTHORS:

Dusan Losic
University of Adelaide
242 PUBLICATIONS **4,676** CITATIONS
SEE PROFILE

Joe G Shapter
Flinders University
268 PUBLICATIONS **3,316** CITATIONS
SEE PROFILE

John Justin Gooding
University of New South Wales
334 PUBLICATIONS **12,066** CITATIONS
SEE PROFILE

Influence of Surface Topography on Alkanethiol SAMs Assembled from Solution and by Microcontact Printing

D. Losic,† J. G. Shapter,*,† and J. J. Gooding*,‡

School of Chemistry, Physics and Earth Science, The Flinders University of South Australia, Adelaide 5001, Australia, and School of Chemistry, The University of New South Wales, Sydney, NSW 2052, Australia

Received October 18, 2000. In Final Form: March 5, 2001

The influence of the topography of the underlying gold surface on the integrity of self-assembled monolayers (SAMs) of hexadecanethiol (HDT) prepared by solution assembly and microcontact printing was assessed using six different gold substrates. The bare substrates were evaluated for roughness and defects using scanning tunneling microscopy (STM). The structural integrity of self-assembled monolayers on these substrates has been evaluated using both surface methods (STM) and electrochemical measurements. Perhaps not surprisingly, the flattest substrates seem to produce the highest quality monolayer. It is surprising to note, however, that the layer quality is not necessarily traceable to a variation in coverage. Despite both the solution-formed and printed SAMs appearing similar in STM images, electrochemical assessment of the SAM integrity indicated the printed SAMs were inferior, forming a less effective passivating barrier with many more pinholes. The quality of printed SAMs could be improved considerably by rolling the inked stamp across the gold surface rather than placing the stamp horizontally onto the substrate. This second printing technique of rolling the stamp across the surface produced SAMs which were still marginally inferior to those formed from solution but were assembled in less than a minute rather than 24 h.

Introduction

Self-assembled monolayers (SAMs) of alkanethiols on gold surfaces possess considerable potential for the development of biosensing interfaces due to their ability to mimic biological membranes,[1] their stability,[2] and their versatility.[2−5] Because of the variety of functions a biorecognition interface is required to fulfill, the versatility is exceedingly important. Certainly any biosensing interface will require the assembly of molecular structures that provide selectivity toward target species. It may however be desirable to intersperse recognition components with other alkanethiols which perform such functions as resist other species absorbing onto the interface[3,6−12] or prevent electroactive species in solution accessing the underlying metal in electrochemical sensing.[13−15] Interspersing the recognition component with a SAM fulfilling other functions can be achieved either by allowing the components to self-assemble onto the interface[1,10,11,14,16] or by controlled patterning of the surface.[12,17−23]

We are interested in using gold electrodes modified with alkanethiols as a basis for electrochemical biosensors where the biorecognition component is an enzyme,[24−27] DNA, or oligopeptides. A long-term goal of this research is to pattern the surface so that arrays of different recognition elements can be immobilized. Of the many emerging methods of patterning interfaces using self-assembled monolayers, perhaps the most popular is microcontact printing. With this emerging technique issues that have been addressed include methods for patterning nonplanar substrates,[28−30] how to decrease the

† The Flinders University of South Australia.
‡ The University of New South Wales.
* Corresponding authors. E-mail Joe.shapter@flinders.edu.au or justin.gooding@unsw.edu.au.

(1) Cornell, B. A.; Braach-Maksvytis, V. L. B.; King, L. G.; Osman, P. D. J.; Raguse, B.; Wieczorek, L.; Pace, R. J. *Nature* **1997**, *387*, 580.
(2) Ulman, A. *An Introduction to Ultrathin Organic Films From Langmuir−Blodgett to Self-Assembly*; Academic Press: London, 1991.
(3) Mrksich, M.; Whitesides, G. M. *Annu. Rev. Biomol. Struct.* **1996**, *25*, 55.
(4) Wink, T.; van Zuilen, S. J.; Bult, A.; van Bennekom, W. P. *Analyst* **1997**, *122*, 43R.
(5) Gooding, J. J.; Hibbert, D. B. *TrAC* **1999**, *18*, 525.
(6) Sieradzki, K.; Brankovic, S. R.; Dimitrov, N. *Science* **1999**, *284*, 138.
(7) Nagaoka, T.; Chen, Z. D.; Okuno, H.; Nakayama, M.; Ogura, K. *Anal. Sci.* **1999**, *15*, 857.
(8) Singhvi, R.; Kumar, A.; Lopez, G. P.; Stephanopoulos, G. N.; Wang, D. I. C.; Whitesides, G. M.; Ingber, D. E. *Science* **1994**, *264*, 696.
(9) Roberts, C.; Chen, C. S.; Mrksich, M.; Martichonok, V.; Ingber, D. E.; Whitesides, G. M. *J. Am. Chem. Soc.* **1998**, *120*, 6548.
(10) Steel, A. B.; Herne, T. M.; Tarlov, M. J. *Anal. Chem.* **1998**, *79*, 4670.
(11) Levicky, R.; Herne, T. M.; Tarlov, M. J.; Satija, S. K. *J. Am. Chem. Soc.* **1998**, *120*, 9787.
(12) Brockman, J. M.; Frutos, A. G.; Corn, R. M. *J. Am. Chem. Soc.* **1999**, *121*, 8044.
(13) Rubinstein, I.; Steinberg, S.; Tor, Y.; Shanzer, A.; Sagiv, J. *Nature* **1988**, *332*, 426.
(14) Flink, S.; Boukamp, B. A.; van den Berg, A.; van Veggel, F. C. J. M.; Reinhoudt, D. N. *J. Am. Chem. Soc.* **1998**, *120*, 4652.
(15) Yang, X.; Kumar, N.; Gooding, J. J.; Hibbert, D. B. *Org. Prep. Proc. Int.* **1999**, *31*, 425.
(16) Hickman, J. J.; Ofer, D.; Laibinis, P. E.; Whitesides, G. M.; Wrighton, M. S. *Science* **1991**, *252*, 688.
(17) Mrksich, M.; Whitesides, G. M. *TIBTECH* **1995**, *13*, 228.
(18) Xia, Y.; Whitesides, G. M. *Angew. Chem., Int. Ed.* **1998**, *37*, 551.
(19) Aizenberg, J.; Black, A. J.; Whitesides, G. M. *Nature* **1998**, *394*, 868.
(20) Delamarche, E.; Bernard, A.; Schmid, H.; Michel, B.; Biebuyck, H. *Science* **1997**, *276*, 779.
(21) Piner, R. D.; Zhu, J.; Zu, F.; Hong, S.; Mirkin, C. A. *Science* **1999**, *283*, 661.
(22) Tender, L. M.; Opperman, K. A.; Hampton, P. D.; Lopez, G. P. *Adv. Mater.* **1998**, *10*.
(23) Xu, S.; Liu, G.-y. *Langmuir* **1997**, *13*, 127.
(24) Gooding, J. J.; Praig, V.; Hall, E. A. H. *Anal. Chem.* **1998**, *70*, 2396.
(25) Gooding, J. J.; Hall, E. A. H.; Hibbert, D. B. *Electroanalysis* **1998**, *10*, 1130.
(26) Gooding, J. J.; Pugliano, L.; Hibbert, D. B.; Erokhin, P. *Electrochem. Commun.* **2000**, *2*, 217.
(27) Gooding, J. J.; Erokhin, P.; Hibbert, D. B. *Biosens. Bioelectron.* **2000**, *15*, 229.
(28) Jackman, R. J.; Wilbur, J. L.; Whitesides, G. M. *Science* **1995**, *269*, 664.

10.1021/la001462t CCC: $20.00
Published on Web 04/24/2001

size of the pattern,[31] strategies for rapidly producing masters for stamps,[18,32] what dimensions give a stable stamp that does not collapse upon itself,[18,33] the order of the printed SAM relative to solution assembled monolayers,[34] methods of inking the stamp,[35] and how the ink is dispersed from the stamp to the substrate.[36] However, considering microcontact printing is a technique in which a monolayer is deposited via direct contact with a surface, it is surprising that there has been no research into the influence of the topography of the gold surface on the integrity of the printed SAM.

The influence of different methods of fabricating metal substrates and how they affect the solution assembly of monolayers of alkanethiols has received a minor amount of attention.[38−43] These studies all investigated gold surfaces with regards to forming a defect-free monolayer. In all studies there seems to be agreement that the important criteria for obtaining a SAM with minimum defects was a surface with the lowest microscopic roughness. By microscopic roughness the authors mean roughness on the order of the adsorbate. Hence, bulk gold surfaces which are rough on a macroscopic scale but contain very few grain boundaries assemble SAMs with less defects than apparently smooth evaporated gold films that contain many more grain boundaries.[38] The role of this microscopic roughness is further highlighted by Porter and co-workers where reductive desorption studies showed that, on gold surfaces with many steps, two stripping peaks were observed due to large thiol domains formed on large gold grains being more stable (and hence requiring a greater potential to desorb) than smaller domains.[43] Hence, gold surfaces with larger grains and fewer grain boundaries are expected to produce more stable SAMs than surfaces with lots of grain boundaries. Techniques for fabricating large atomically flat gold surfaces for SAMs and immobilization of biomolecules have also been reported as very promising, but how the SAM integrity compares to other methods of fabricating gold has not been evaluated.[44−47]

In this paper we characterize gold surfaces fabricated in six different ways and explore how the surface topography influences the integrity of SAM formed on these surfaces. Initially the influence of the gold surfaces is characterized with SAMs formed from solution. This characterization then serves as a frame of reference for the investigation of the influence of the gold topography on microcontact printed SAMs. To develop a basis for the discussion of our results, we first describe STM experiments on different bare gold substrates, revealing microscopic surface topography. The integrity of the SAMs formed on these surfaces is then characterized using electrochemical methods. The electrochemical assessment exploits that long-chain alkanethiols act as physical barriers, preventing molecules in solution from closely approaching the underlying gold substrate.[48] The alkanethiol used was the commonly chosen hexadecanethiol (HDT), thus allowing direct comparison to previous studies. SAMs were investigated to measure passivation to ion permeation (electrochemical capacitance),[48−50] blocking heterogeneous electron transfer,[51−56] electrochemical reduction of gold oxide,[48,57] and reductive desorption.[39,58,59] Described methods have been used to assess SAM film structural integrity on different gold substrates to correlate those results with STM results on bare gold substrates.

Experimental Section

Materials. Gold foil (99.95%), 25 mm × 25 mm, was supplied from Peter W. Beck Pty. Ltd. Adelaide, Australia. Gold wire (0.25 mm diameter, 99.999%), Ti wire (0.1 mm diameter, 99.999%), 1-hexadecanethiol (HDT), and (3-mercaptopropyl)trimethoysilane (MPS) were purchased from Aldrich. *p*-Benzoquinone, potassium ferricyanide, potassium chloride, potassium dihydrogen orthophosphate, dipotassium hydrogen orthophosphate, and potassium hydroxide were supplied from Ajax Chem Pty. Ltd. (Sydney, Australia). The poly(dimethyl)siloxane (PDMS), brand name Silgard 184, was obtained from Dow Corning, Midland, MI. Other chemicals were of highest quality commercially available and were used without further purification. All aqueous solution were prepared with Milli-Q grade water.

Preparation of Gold Substrates. Six different gold substrates were used for this study. They are (A) bulk gold, (B) gold on mica evaporated at room temperature (Au−mica), (C) gold on mica, evaporated with the mica at 300 °C followed by annealing (Au−mica annealed), (D) flat gold fabricated by stripping gold film from mica template (flat gold), (E) gold on glass coated with Ti (Au−Ti−glass), and (F) gold on glass coated with MPS (Au−MPS−glass). The preparation of each of these substrates is described in detail below:

(A) Bulk Gold. Bulk gold substrate was prepared by cutting gold foil into 7 mm × 15 mm pieces that was then polished to a mirror finish using 1, 0.3, and 0.05 μm alumina/water slurry on polishing cloths. An ultrasonic cleaner was employed for removal of residential alumina trapped at the surface. The gold surface was cleaned with "piranha" solution comprising 1:3 (v/v) 30% H_2O_2 and concentrated H_2SO_4 for 2 min and then rinsed with copious amounts of water followed by ethanol. **(Warning: piranha solution reacts violently with organic material**

(29) Xia, Y.; Qin, D.; Whitesides, G. M. *Adv. Mater.* **1996**, *8*, 1015.
(30) Rogers, J. A.; Jackman, R. J.; Whitesides, G. M. *J. Microelectromech. Syst.* **1997**, *6*, 184.
(31) Xia, Y.; Whitesides, G. M. *Adv. Mater.* **1995**, *7*, 471.
(32) Qin, D.; Xia, Y.; Whitesides, G. M. *Adv. Mater.* **1996**, *8*, 917.
(33) Delamarche, E.; Schmid, H.; Michel, B.; Biebuyk, H. *Adv. Mater.* **1997**, *9*, 741.
(34) Larsen, N. B.; Biebuyck, H.; Delamarche, E.; Michel, B. *J. Am. Chem. Soc.* **1997**, *119*, 3017.
(35) Libioulle, L.; Bietsch, A.; Schmid, H.; Michel, B.; Delamarche, E. *Langmuir* **1999**, *15*, 300.
(36) Delamarche, E.; Schmid, H.; Bietsch, A.; Larsen, N. B.; Rothuizen, H.; Michel, B.; Biebuyck, H. *J. Phys. Chem. B* **1998**, *102*, 3324.
(37) Widrig, C. A.; Chung, C.; Porter, M. D. *J. Electroanal. Chem.* **1991**, *310*, 335.
(38) Creager, S. E.; Hockett, L. A.; Rowe, G. K. *Langmuir* **1992**, *8*, 854.
(39) Walczak, M. M.; Alves, C. A.; Lamp, B. D.; Porter, M. D. *J. Electroanal. Chem.* **1995**, *396*, 103.
(40) Guo, L.-H.; Facci, J. S.; McLendon, G.; Mosher, R. *Langmuir* **1994**, *10*, 4588.
(41) Hou, Z.; Abbott, N. L.; Stroeve, P. *Langmuir* **1998**, *14*, 3287.
(42) Hou, Z.; Dante, S.; Abbott, N. L.; Stroeve, P. *Langmuir* **1999**, *15*, 3011.
(43) Wong, S.-S.; Porter, M. D. *J. Electroanal. Chem.* **2000**, *485*, 135.
(44) Hegner, M.; Wagner, P.; Semenza, G. *Surf. Sci.* **1993**, *291*, 39.
(45) Wagner, P.; Hegner, M.; Guntherodt, H. J.; Semenza, G. *Langmuir* **1995**, *11*, 3867.
(46) Wagner, P.; Hegner, M.; Kernen, P.; Zaugg, F.; Semenza, G. *Biophys. J.* **1996**, *70*, 2052.
(47) Wagner, P.; Zaugg, F.; Kernen, P.; Hegner, M.; Semenza, G. *J. Vac. Sci. Technol. B* **1996**, *14*, 1466.
(48) Finklea, H. O. *Electroanal. Chem.* **1996**, *19*, 109.
(49) Xu, J.; Li, H.-L. *J. Colloid Interface Sci.* **1995**, *176*, 138.
(50) Sondag-Huethorst, J. A. M.; Fokkink, G. J. *Langmuir* **1995**, *11*, 2237.
(51) Chidsay, C. E. D.; Loiacono, D. N. *Langmuir* **1990**, *6*, 682.
(52) Porter, M. D.; Bright, T. B.; Allara, D. L.; Chidsay, C. E. D. *J. Am. Chem. Soc.* **1987**, *107*, 3559.
(53) Che, G.; Li, Z.; Zhang, H.; Cabrera, C. R. *J. Electroanal. Chem.* **1998**, *453*, 9.
(54) Amatore, C.; Saveant, J. M.; Tessier, D. *J. Electroanal. Chem.* **1983**, *147*, 39.
(55) Takehara, K.; Takemura, H.; Ide, Y. *Electrochim. Acta* **1994**, *39*, 817.
(56) Diao, P.; Jiang, D.; Cui, X.; Gu, D.; Tong, R.; Zhong, B. *J. Electroanal. Chem.* **1999**, *464*, 61.
(57) Sabatini, E.; Rubinstein, I. *J. Phys. Chem.* **1987**, *91*, 6663.
(58) Walczak, M. M.; Popenoe, D. D.; Deinhammer, R. S.; Lamp, B. D.; Chung, C.; Porter, M. D. *Langmuir* **1991**, *7*, 2687.
(59) Weisshaar, D. E.; Walczak, M. M.; Porter, M. D. *Langmuir* **1993**, *9*, 323.

and has been known to explode when stored in closed containers!) A final check of surface cleanliness was obtained by placing the electrode in 0.5 M H_2SO_4 and scanning the potential between −0.5 and 1.5 V vs Ag/AgCl at scan rate of 100 mV s^{-1} until a reproducible scan was recorded (typically 30 min). Following this cycling, the gold electrodes were rinsed with water and dried under nitrogen before the self-assembling procedure.

Thin gold film substrates were all prepared by thermal vacuum evaporation of about 3000 Å of gold (measured using a film thickness monitor) onto either freshly cleaved muscovite mica or glass (microscopes slides). The turbomolecular-pumped evaporator's base pressure was below 1×10^{-5} Torr.

(B) Au−Mica. Evaporation of gold on mica (sheet 50 mm × 50 mm) at room temperature was performed as soon as the background pressure reached the evaporator base pressure.

(*C) Au−Mica Annealed.* Mica was heated using a specially designed heater block with temperature feedback control through a thermocouple placed on mica face. Mica substrates were heated to 300 °C for 4 h before the evaporation and held at 300 °C during the evaporation. Resulting films were annealed for between 4 and 16 h after evaporation at 300 °C. The sample was cooled under vacuum to less than 60 °C prior to removal from the evaporation chamber. This procedure was used to decrease mica impurities and promote preferential epitaxial gold growth of the Au (111) face.[40,60,61]

(D) Flat Gold. Large atomically flat gold substrates were stripped from the mica template using a procedure described by Shapter.[62] The basic idea is to use the first gold atomic layer which has been deposited directly on the mica rather than the top gold surface. Using the gold layer contacting the mica takes advantage of the atomic flatness of the mica. These mica/gold/glass substrates can be stored as stripping precursors for several months without loss of quality. After each stripping the conductivity of the surface was checked, and finally the surface was examined using a standard stereomicroscope.

Two different methods were used to promote adhesion of gold to glass. Microscope slides (25 mm × 75 mm) were cleaned with a piranha solution for 5 min and thoroughly rinsed with deionized water, dried with flowing nitrogen, and then oven-dried at 105 °C for 20 min. These slides were used to make Au−Ti−glass and glass−MPS−Au substrates.

(E) Au−Ti−Glass. A 200 Å titanium underlayer followed by 3000 Å of gold was deposited by vacuum evaporation. The surface deposition temperature was 150−200 °C.

(F) Au−MPS−Glass. Glass slides were coated with monolayers of 3-mercaptopropyltrimethoxysilane (MPS) using a procedure described elsewhere.[24] Cleaned microscopic slides were placed in 95:5 (v/v) methanol/water solution with 0.5% of MPS. The silane is hydrolyzed and condenses with the surface −OH groups to form a silane polymer at the surface with exposed thiol groups. The slides were stored in the MPS solution for minimum of 24 h to allow sufficient time for polymerization of the silane. Subsequently, the slides were sonicated for 2 min in ethanol to remove excess free polymer and then placed in the oven for 3 h or more at 150 °C. Upon removal from the oven, the slides were transferred to the evaporator and heated to 150−200 °C during evaporation and annealed under vacuum at 200−250 °C for 2−4 h after evaporation.

After evaporation, the gold/glass substrates (Au−Ti−glass and Au−MPS−glass) were cut with a diamond tipped stylish to 1 cm × 2 cm area and used immediately.

The electrochemical roughness (the electrochemically accessible area divided by the geometric area) of the gold substrates was measured from CVs of $K_3Fe(CN)_6$ in 0.2 M KCl using the Randles−Sevcik equation. The literature value for the diffusion coefficient of ferricyanide of 7.6×10^{-6} cm^2 s^{-1} at 25 °C[63] was used.

Self-Assembled Monolayer Modification—Solution Assembly. Gold substrates were immersed in a solution of 10 mM 1-hexadecanethiol (HDT) in absolute ethanol immediately after preparation. SAM formation proceeded for a minimum of 24 h at 25 °C. The Au−HDT-coated substrates were rinsed in ethanol and then water prior to investigating the integrity of the SAM.

Self-Assembled Monolayer Modification—via Microcontact Printing. Unpatterned poly(dimethyl)siloxane flat stamps were prepared from Silgard 184 (Dow Corning, Midland, MI) and cured at least 12 h at 60 °C on flat mica sheets. Inking of the stamps was performed using one drop (1 μL mm^{-2} of stamp) of the same 10 mM thiol solution as in the solution work. The drop was removed after 30 s under a stream of nitrogen. The stamp was then used immediately. The stamp was placed horizontally on the surface. The time of contact was 2−3 s. Additionally, a "rolling" procedure of stamping has been used in an attempt to improve SAM integrity. Stamp contact with substrates was initiated by rolling from one end to the other until the entire stamp was in contact with the substrate. Each printed SAM was used 10 min after preparation.

Surface Characterizations. *Scanning Tunneling Microscopy (STM).* STM measurements of the gold substrates were made under ambient conditions using a Nanoscope II (Digital Instruments). This microscope is a somewhat older version, and hence limited tunneling currents are reachable. In practice, this means that reliable imaging can be done above 100 pA. All bare substrate images were obtained in the constant current mode using mechanically cut Pt/Ir tips. A sample bias voltage was typically +0.2 V and tunneling current set point of 3 nA. SAM-modified substrate images were typically performed using about +1.0 V and a few hundred picoamps. *Z*-calibration was confirmed by measurement of Au(111) step heights. All images presented are unfiltered data. Roughnesses were calculated using surface analysis software. Two scales of images were typically obtained for each gold substrate: small scale images usually about 100 nm × 100 nm and large scale images greater than 1 μm × 1 μm in size. Generally, five different areas on at least three samples of each type substrate were examined.

For a quantitative analysis of the six surfaces, we have used the STM to calculate three main parameters by which roughness is characterized, namely, R_a, R_{rms}, and R_{max}. Roughness (R_a) is the arithmetic average surface roughness, and it is determined using the graphical centerline method. Basically, this represents the mean value of the roughness curve relative to the center line. R_{rms} (standard deviation) is the standard deviation of *Z* values between the reference markers. R_{max} (maximum height) is the difference in height between the highest and lowest points on the cross-sectional profile relative to the center line (not the roughness curve) over the length of the profile.

Electrochemical Cell and Instrumentation. All electrochemical experiments and were performed using a Power Lab, model 400 S (AD Instruments, Sydney, Australia) computer-controlled electrochemical system at room temperature. All potentials are quoted relative to a Ag/AgCl reference electrode. A platinum wire auxiliary electrode completed the three-electrode configuration. Electrochemical measurements were performed in specially designed Plexiglas electrochemical cell which defined the active area of electrode using an O-ring pressed against the examined gold substrates. The area exposed to the electrolyte solution was 0.075 ± 0.005 cm^2. Each substrate provides two or four spots for testing. Electrolyte solutions were purged with argon for at least 30 min prior to measurement and blanketed in argon throughout the experiments.

Cyclic Voltammetry (CV). Each SAM-modified gold surface was interrogated using four different voltammetric experiments. The order of assessment for each modified electrode was (1) the measurement of a CV in simple electrolyte, (2) measurement of heterogeneous electron transfer using ferricyanide, (3) electrochemical reduction of gold oxide, and (4) reductive desorption. Quoted results of the electrochemical characterization are averages from five gold preparations and five HDT-modified samples with four testing spots used for each substrate. Only samples with good integrity films were included in the results.

Cyclic voltammetry in simple electrolytes and electrochemical capacitance measurement were performed in 1 M KCl and phosphate buffer (pH 7.00). Steady-state voltammograms of different gold substrates coated with HDT were obtained in a potential range of −0.5 to 0.8 V with scan rates of 10 and 100 mV s^{-1}.

(60) Chidsey, C. E. D.; Loicono, D. N.; Sleator, T.; Nakahara, S. *Surf. Sci.* **1988**, *200*, 45.
(61) Putman, A.; Blackford, B. L.; Jericho, M. H.; Watanabe, M. O. *Surf. Sci.* **1989**, *217*, 276.
(62) Shapter, J. Provisional Patent Number PQ7662/00.
(63) Stackelberg, M. V.; Pilgram, M. Z. *Electrochem.* **1953**, *57*, 342.

The charging current at 0.0 V (μA s^{-1}) was calculated recorded from CV's while total charge Q (μC) was calculated by integration of the charging current. All parameters were normalized to unit electrode area. The ratio between the total charge of HDT-coated electrode and bare gold electrode (Q_{HDT}/Q_{Au}) was used to obtain a film "ion barrier factor" ($1 - Q_{SAM}/Q_{bare}$).[64]

Heterogeneous electron-transfer measurements for the assessment of the passivating ability of the films were conducted in 1 mM $K_3Fe(CN)_6$ in 0.2 M KCl. Applied potential windows of -0.5 to $+0.8$ V with scan rates between 25 and 200 mV s^{-1}. The CVs with ferricyanide also provide an indication of the extent of defects and pinholes in the HDT SAMs via comparison of the theoretical and apparent electron-transfer rate. The apparent electron-transfer rate constant (k_{app}) is calculated using methods reported elsewhere[56,57,65] where the electron-transfer resistance (R_T) is obtained from the linear, low overpotential regions of the CV's.

Electrochemical stripping of gold oxide was performed in 0.1 M H_2SO_4 at potentials of -0.5 to 1.5 V at scan rates of 100 mV s^{-1}. The integrated charge, Q (μC cm^{-2}), under the oxide removal peak of SAM-modified electrode was used as a measure of the total fractional pinhole area, $1 - \theta$ (where θ is the SAM coverage), using charge at bare gold for each substrate as described elsewhere.[57] Stripping was followed by an additional scan in the same voltage range to verify the total removal of the oxide in the first scan with the second reduction scan used as basis for calculations. Additionally, repeated cycling for up to 25 cycles was used as a guide to the robustness of the SAMs on each substrate.

Reductive desorption of SAM-modified electrodes was performed in 0.5 M KOH in a potential window -0.2 to -1.4 V at 100 mV s^{-1}. The value of passed charge, Q (μC cm^{-2}), is determined from the CVs by integration of the area under the reduction peak after accounting for the charging current and roughness and used for calculating of HDT coverage, Γ (nmol cm^{-2}), as described.[39,58,59]

Results and Discussion

Surface Characterization of Gold Substrates by STM. Figure 1 shows STM images of the various substrates while Figure 2 shows corresponding cross sections from those images. Table 1 summarizes the roughness data obtained from the various substrates. Table 1 shows that, regardless of the method of measuring the surface roughness, the order from smoothest to roughest substrate was flat gold (D), Au−mica annealed (C), Au−MPS−glass (F), Au−Ti−glass (E), bulk gold (A), and Au−mica (B).

Table 1 also provides information regarding the grain size and the extent of imperfections. The grain size and flat areas were determined from the cross sections. Grain size was defined by the distance between their boundaries (defined as greater than a 2 nm slope over 10 nm). A flat area is regarded as a region where the roughness is less than 2 nm over a horizontal distance of at least 10 nm. The percentage area of imperfections is calculated using

$$\%\ \text{imperfections} = \left(1 - \frac{\text{total flat area}}{\text{total area}}\right) \times 100$$

The grain size data in Table 1 indicates the higher proportion of small gold grains, the rougher the surface and the more grain boundaries and imperfections. The importance of the surface preparation technique is highlighted by Figure 1B,C where in both cases the gold is evaporated onto mica. With the mica gold (Figure 1B) the cold evaporation results in many nucleation sites. A variety of nucleation sites are still visible at the end of the evaporation as the low deposition temperature restricts the gold mobility, preventing coalescence into a single grain. The resultant surface has a large number of visible grain boundaries and is exceedingly rough. Evaporating onto the same surface at 300 °C allows the gold to migrate on the surface, resulting in a much smoother surface with larger grains and fewer defects.

Flat gold (D) yielded a very smooth surface with large atomically flat areas and the occasional atomic step. Flat gold shows the (111) crystal orientation over about 70% of the substrate as evidenced by the triangular faceting characteristic of this plane. Much of the rest of the surface is still very flat but does not reveal an obvious crystal orientation. The surface is probably slightly amphorous in these areas. The smoothness of this gold surface is apparent in Figure 1D where a single step is observed. Figure 2D reveals that the maximum variation in height over the surface, R_{max}, is of the order of a single nanometer in 1000 nm^2. Larger scale AFM images reveal deep, sparsely spaced large holes in the gold substrate. These result from the stripping process and correspond to observed impurities on the mica substrate from which the sample is separated. The electrochemical roughness measurement of almost 1 shows that these few holes make only a very minor contribution to roughening the surface.

The Au−mica annealed (C) surface also contains near atomically flat regions, but overall the surface is significantly rougher and contains many more defects per unit area that the flat gold. In contrast, the other four substrates show very few if any atomically flat regions.

STM Images of Gold Substrates Modified with HDT SAMs. The influence of the gold surface topography on the integrity of SAMs formed from solution was initially investigated using STM. The images obtained fell into two basic categories. Figure 3 shows representative images of each category. An apparently continuous SAM was obtained on the smoother gold surfaces, including flat gold, Au−mica annealed, Au−MPS−glass, and Au−Ti−glass (see Figure 3a). In higher resolution images of the SAM-modified flat gold image (Figure 3b), the "channels" observed have been seen in other work[66] and are due to domain boundaries in the layer. Cross-sectional analysis of the image confirms this assignment. In contrast, on the two particularly rough surfaces, bulk gold and Au−mica, holes were evident throughout the image which appear to be holes in the SAM (Figure 3c), although it should be stressed there is no definitive way to differentiate between holes in the gold substrate and the SAM.

The printed SAMs, whether printed or rolled, produced very similar images to the solution-formed SAMs. The similarity of the STM images when printed and formed from solution was consistent with the observations of Larsen et al.,[34] who showed via STM images and wetting studies that provided the stamp was inked with 10 mM or greater of alkanethiol, SAMs were indistinguishable from those formed in solution are obtained.

In the case of both the solution-formed SAMs and the printed SAMs, subtle differences in the integrity of the SAMs on the different gold surfaces could not be elucidated due to the image resolution. However, our inability to get to tunneling currents on the order of a few picoamps with the STM used prevented the obtaining of higher resolution images reported by Larsen and others.[34] Therefore, to obtain a greater understanding of the influence of the gold surface topography on the integrity of both solution-formed and printed SAMs, electrochemical methods were employed.

Electrochemical Characterization of SAM Monolayers on Gold. Each SAM-modified gold surface was

(64) Wang, J.; Paz, J. L. P.; Jiang, M. *Langmuir* **1999**, *15*, 1884.
(65) Diao, P.; Jiang, D. L.; Cui, X. L.; Gu, D. P.; Tong, R. T.; Zhong, B. *Bioelectrochem. Bioenerg.* **1999**, *48*, 469.
(66) Delamarche, E.; Michel, B.; Kang, H.; Gerber, Ch. *Langmuir* **1994**, *10*, 4103.

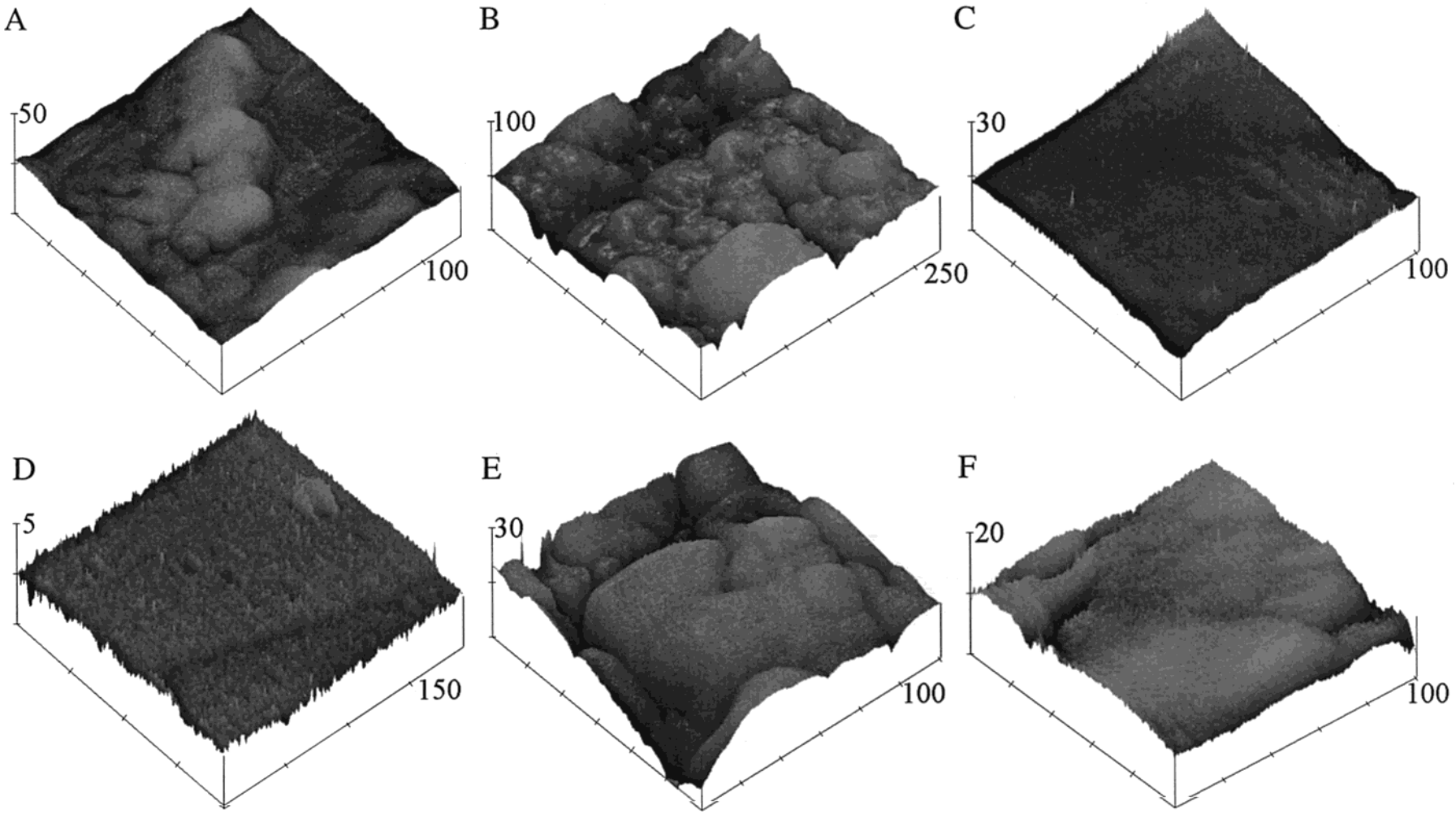

Figure 1. STM images of various bare gold substrates: (A) bulk gold, (B) Au−mica, (C) Au−mica annealed, (D) flat gold, (E) Au−Ti−glass, and (F) Au−MPS−glass. All dimensions given in nm.

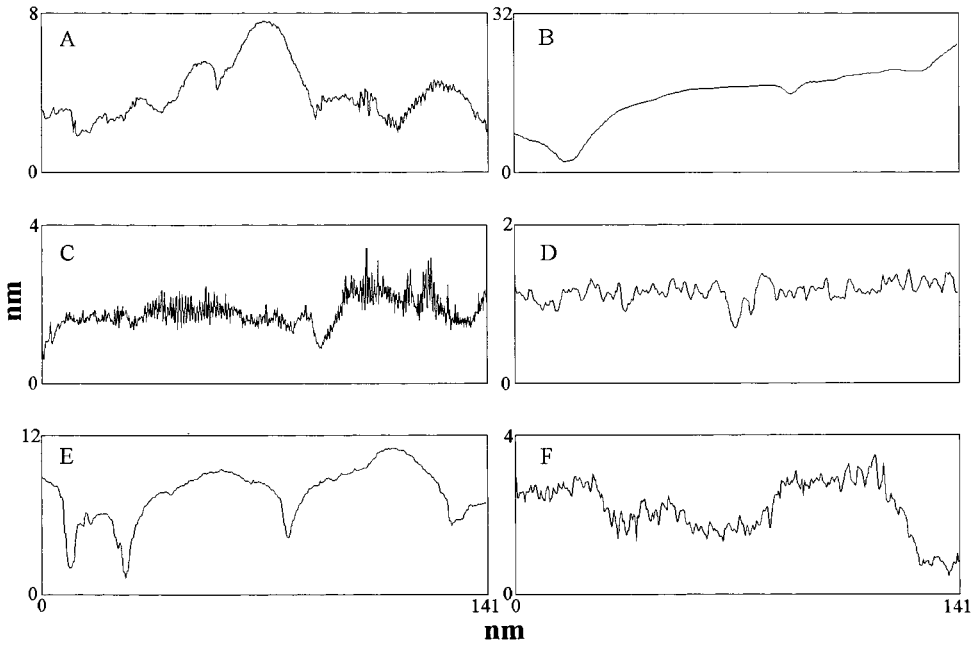

Figure 2. Cross sections of the images in Figure 3. All cross sections are taken for a 100 nm × 100 nm section of the image. In the cases where the images in Figure 3 are larger, the central section of the image is used. All cross sections are from the upper left corner of the image to the lower right. Note the changes in scale for *y*-axes.

Table 1. Summary of Topography of Different Gold Substrates

gold substrate	grain size, av (1000 nm^2)	flat areas, av (1000 nm^2)	imperfections density (%)	roughness 100 × 100 nm			electrochemical roughness
				R_{rms} (nm)	R_a (nm)	R_{max} (nm)	
bulk gold	1−2	0.7−1	40−55	5.1 ± 0.5	3.5 ± 0.5	30 ± 5	1.54 ± 0.01
mica gold	0.5−1	<0.5	70−85	7.7 ± 0.3	5.6 ± 0.3	50 ± 10	1.62 ± 0.02
mica gold (ann)	20−40	15−25	2−4	0.32 ± 0.07	0.25 ± 0.07	4 ± 1	1.11 ± 0.05
flat gold	40−80	40−80	0.5−1	0.12 ± 0.03	0.09 ± 0.03	1.2 ± 0.2	1.05 ± 0.04
Au−Ti−glass	2−4	1−1.5	30−40	2.1 ± 0.5	1.8 ± 0.4	15 ± 5	1.37 ± 0.06
Au−MPs−glass	5−10	3−5	10−20	0.95 ± 0.05	0.75 ± 0.05	7 ± 2	1.26 ± 0.05

interrogated using four different voltammetric experiments to gain information regarding the monolayer integrity.

(1) The interfacial capacitance was determined from CVs measured in simple electrolyte. The interfacial capacitance serves as a probe of ion permeability through the SAM[48] and therefore provides an indication of how "close-packed" and defect free the monolayer is.

(2) An indication of the size and number of defects was gained by measuring the heterogeneous electron-transfer rate using ferricyanide. Three different types of voltammetric shape are anticipated depending on the quality of the SAM: (a) peak-shaped curves reminiscent of a macroelectrode suggests planar diffusion to closely spaced defect sites or large bare areas; (b) a sigmoidal voltammetric response is characteristic of a microelectrode arrays, hence suggesting radial diffusion to broadly spaced small defect sites; and (c) exponentially shaped curves which, according to Amatore[54] and Finklea,[48] indicate the current is derived from electron transfer across a densely packed polymethylene chain (tunneling process). A more quantitative estimate of the relative number of defects between the different substrate is obtained by measuring the apparent rate constant of electron transfer.[56,65] If there is no obvious redox activity in the CV, charge transfer can occur either via tunneling across the well-ordered SAM or tunneling across thin SAM layers at collapsed sites. Diao et al.[56,65] have used variations in the apparent heterogeneous electron-transfer rate constant, k_{app}, as an indication of the number of collapsed sites. k_{app} can be obtained using

$$k_{app} = RT/(F^2 R_t c°)$$

where R is the gas constant, T the temperature, F the Faraday constant, R_t the charge-transfer resistance obtained from the CV at low overpotentials, and $c°$ the concentration of the redox couple.

(3) The total fraction of defects in SAM-modified gold substrates can be determined by the oxidation of any bare gold and then stripping of the gold oxide. The ratio of integrated peak areas of the SAM-modified and bare gold electrodes of the same surface area yields $1 - \theta$ (total fractional pinhole area), with θ being the fraction of monolayer coverage.[48,57]

(4) Finally, the surface coverage of HDT (Γ) was determined by reductively desorbing the SAM.[38,58,59] SAMs desorb quantitatively from gold at negative potentials in strongly alkaline electrolytes.

Tables 2 and 3 summarize this electrochemical data for the various substrates that were modified with HDT via solution assembly and by microcontact printing, respectively.

Solution Assembled SAMs. The investigation of the barrier each solution assembled SAM provides to ion permeability (Table 2) shows that the rougher the underlying gold surface, the higher interfacial capacitances and hence the more defects there are in the SAM. Heterogeneous electron-transfer studies using ferricyanide reveal the extent to which these defects isolate the electrode from the bulk solution. Figure 4 shows a wide

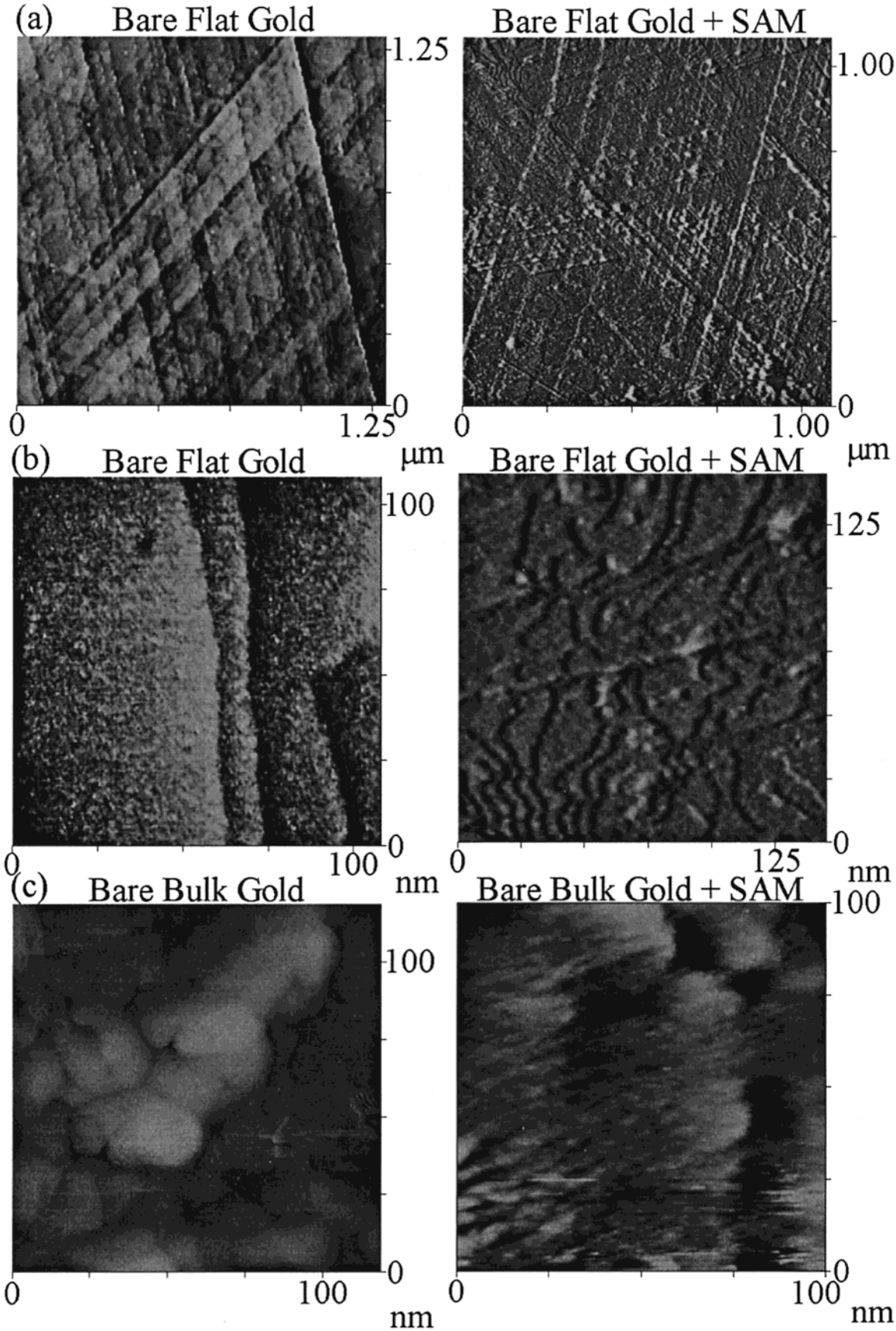

Figure 3. STM Images of SAM-modified flat gold: (a) bare flat gold and SAM-modified flat gold; (b) as for (a) except at higher resolution; (c) bulk gold and SAM-modified bulk gold.

variability in the blocking ability to ferrcyanide electrochemistry of SAMs on the six different surfaces. At one extreme is the peak-shaped CVs on the roughest mica gold and bulk gold, indicating the SAMs contain many defects. At the other extreme are the smooth flat gold and Au−mica (annealed) with consistently exponential shaped

Table 2. Electrochemical Properties of SAM-Modified Gold Substrates (Solution Deposition) (Error Bar ± σ of 3−5 Results)

	gold substrates					
	bulk gold	mica gold	mica gold (ann)	flat gold	Au−Ti−glass	Au−MPS−glass
	SAM from Solution					
ion barrier factor $(1 - Q_{SAM}/Q_{bare})$	0.984 ± 0.003	0.975 ± 0.005	0.992 ± 0.002	0.995 ± 0.002	0.985 ± 0.005	0.990 ± 0.004
CV curves	peak-shaped to sigmoidal	peak-shaped to sigmoidal	exponential	exponential	peak-shaped to sigmoidal	sigmoidal to exponential
k_{app}/cm s^{-1}	$(5.1 \pm 0.5) \times 10^{-6}$	$(5.3 \pm 0.4) \times 10^{-5}$	$(1.8 \pm 0.3) \times 10^{-7}$	$(1.1 \pm 0.5) \times 10^{-7}$	$(3.3 \pm 0.2) \times 10^{-6}$	$(2.4 \pm 0.2) \times 10^{-6}$
pinhole fraction, $1 - \Theta$	0.0044 ± 0.0003	0.0095 ± 0.0005	undetectable to 0.0007	undetectable to 0.0007	0.0032 ± 0.0005	0.0015 ± 0.0003
coverage (Γ)/ nmol cm^{-2}	0.73 ± 0.05	0.74 ± 0.03	0.82 ± 0.04	0.81 ± 0.04	0.79 ± 0.02	0.75 ± 0.06

Table 3. Electrochemical Properties of SAM-Modified Gold Substrates (μCP Deposition) (Error Bar ± σ of 3−5 Results)

	gold substrates					
	bulk gold	mica gold	mica gold (ann)	flat gold	Au−Ti−glass	Au−MPS−glass
	Printed SAM (Horizontal)					
ion barrier factor $(1 - Q_{SAM}/Q_{bare})$	0.864 ± 0.007	0.820 ± 0.01	0.950 ± 0.005	0.946 ± 0.005	0.905 ± 0.007	0.917 ± 0.005
CV curves	peak-shaped	peak-shaped	peak-shaped	peak-shaped	peak-shaped	peak-shaped
k_{app}/cm s^{-1}	$(1.1 \pm 0.5) \times 10^{-3}$	$(1.3 \pm 0.4) \times 10^{-3}$	$(4.8 \pm 0.3) \times 10^{-4}$	$(4.2 \pm 0.5) \times 10^{-4}$	$(3.3 \pm 0.20) \times 10^{-3}$	$(2.4 \pm 0.2) \times 10^{-3}$
pinhole fraction, $1 - \Theta$	0.05 ± 0.008	na	0.009 ± 0.0005	0.009 ± 0.0005	0.015 ± 0.002	0.011 ± 0.001
coverage (Γ)/ nmol cm^{-2}	0.65 ± 0.15	0.5 ± 0.1	0.73 ± 0.05	0.73 ± 0.05	0.71 ± 0.03	0.72 ± 0.05
	Printed SAM (Rolling)					
ion barrier factor $(1 - Q_{SAM}/Q_{bare})$	0.915 ± 0.02			0.977 ± 0.005		
CV curves	peak-shaped to sigmoidal			sigmoidal to exponential		
k_{app}/cm s^{-1}	$(3.3 \pm 0.5) \times 10^{-4}$			$(3.8 \pm 0.5) \times 10^{-5}$		
pinhole fraction, $1 - \Theta$	0.006 ± 0.001			0.003 ± 0.0007		
coverage (Γ)/ nmol cm^{-2}	0.71 ± 0.07			0.76 ± 0.05		

CVs, indicating the SAMs provide an effective barrier to heterogeneous electron transfer. The apparent rate electron transfer k_{app} allows a more quantitative estimate of this barrier each SAM provides. As is evident from Table 2, there is a dramatic decrease in rate of electron transfer as the substrate becomes smoother. The decrease in k_{app} is consistent with fewer defects in the SAM. The measurement of the number of defects in the SAMs showed that in the case of flat gold and Au−mica annealed the pinhole fraction was too small to reliably measure. In contrast, about 1% of the roughest surface, mica gold, was covered with pinholes.

The electrochemical assessment of the solution assembled SAMs shows the integrity of the monolayer decreases from flat gold (D), Au−mica annealed (C), Au−MPS−glass (F), Au−Ti−glass (E), bulk gold (A), and Au−mica (B). The variation in the integrity is not however definitively equated to the amount of HDT adsorbed. The calculated surface coverages of alkanethiol in the range 0.73−0.82 nmol cm^{-2} is consistent with previously reported surface coverages.[37] The reductive desorption studies show that there is little difference in the amount of thiol adsorbed despite more than an order of magnitude change in R_{rms}. This observation confirms that it is the quality of the resultant SAM, rather than the amount of adsorbate, which is responsible for the better passivating ability of SAMs formed on the smoother substrates. These results are therefore consistent with those of Creager et al.[38] that the imperfections, steps, and roughness play a significant role in determining the quality of the resultant SAM. The STM data (Table 1) show that the smoother substrates have larger grain sizes with fewer imperfections. Hence, the SAMs formed on these surfaces have fewer defects.

The more continuous SAMs formed on the smoother substrates also appear to be more robust with regard to resisting desorption. During the measurement of the pinhole fraction, the high positive potentials (+1.5 V) required to oxidize the bare gold in the pinholes, may cause some oxidative desorption of the SAM. By repeatedly cycling between −0.5 and +1.5 V the resistance of the SAM to this electrochemical degradation can be assessed. Figure 5 shows the fraction of pinholes observed as a function of number of cycles between −0.5 and +1.5 V. Results are shown for the first 10 cycles, and the trend of more robust SAMs on the smoother surfaces is clear. Up to 40 cycles were used for some SAMs with the flat substrates maintaining their integrity for the entire experiment. We propose this greater robustness of the SAMs on the smoother substrates is because the large atomically flat regions on flat gold and Au−mica (annealed) allow large areas of SAM where hydrophobic interactions can operate over the entire length of the alkyl chains. Such hydrophobic interactions would provide these domains with greater resistance to degradation than poorly associated alkanethiols because to disrupt the SAM in these regions will require either disturbing the hydrophobic forces or removing the entire domain as a single sheet.

Reductive desorption experiment results support the idea that more robust SAMs with larger domains are formed on the smoother surfaces. During these experiments the electrode was cycled several times between −0.2 and −1.4 V. In all cases, on the first cycle a large peak due to the desorption of the HDT is observed. On the second cycle there is a smaller but distinct peak at the same place, −1.1 V for the solution-formed SAM on flat gold. The presence of the peak on the second scan indicates oxidative readsorption of a significant portion of the SAM as the

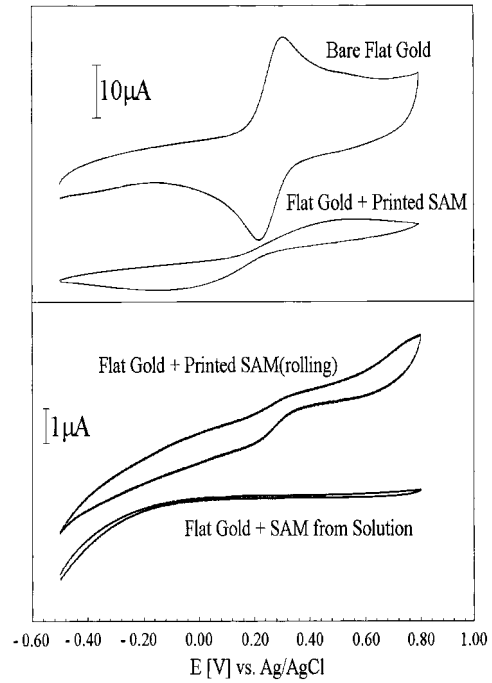

Figure 4. Typical CV's obtained in electron-transfer experiments for flat gold showing different shaped features. CV's obtained using a redox probe of 1 mM $K_3Fe(CN)_6$ in 0.2 M KCl and scan rate of 0.1 V s^{-1}.

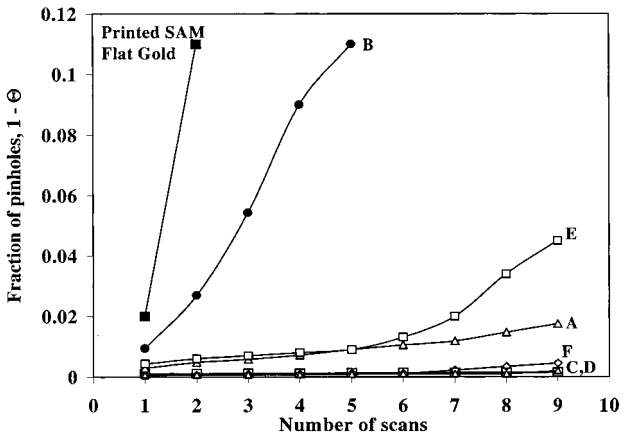

Figure 5. Stability of HDT SAMs assembled from solution as a function of the number of CV cycles for each gold substrate. The labels A to F refer to each gold surface as in Figure 3.

potential sweeps back to more positive potentials during the first cycle. With subsequent cycles the size of the reductive desorption peak continues to decrease as less and less alkanethiol readsorbs onto the gold surface with each sweep back to positive potentials. Similar behavior is observed with the Au−mica annealed surface. In contrast with the very rough Au−mica there is significantly less readsorption which is consistent with the observations of the effects of surface roughness on thiol readsorption by Yang et al.[67] The SAMs on surfaces of intermediate roughness do show intermediate amounts of readsorption. In the second cycles two peaks are observed, both more positive in potential than the original stripping peak, which is consistent with those observed by Walczak et al.[39,58]

The readsorption of the alkanethiol after being reductively desorbed can be attributed to alkanethiol which has not diffused away from the electrode when the

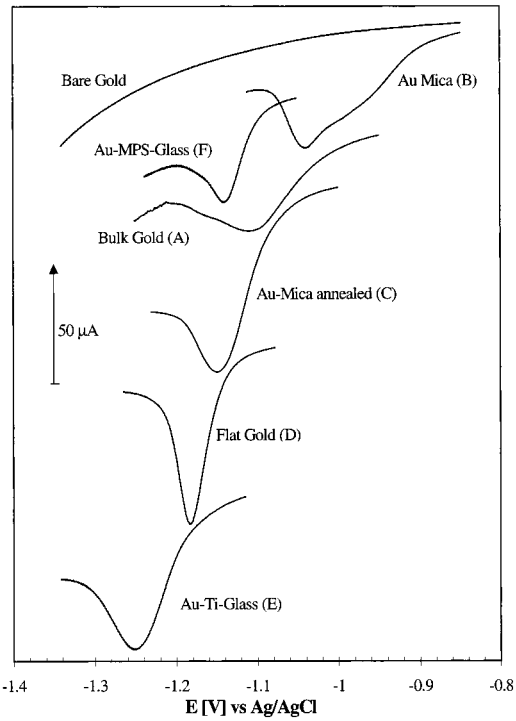

Figure 6. Reductive desorption CV peaks for various gold substrates coated with SAM (first cycle). All recorded in 0.5 M KOH at scan speeds of 100 mV s^{-1} except Au−MPS−glass (F) which is recorded at 5 mV s^{-1}.

potential sweeps back to where the thiols can adsorb stably onto the gold. If a domain of alkanethiol desorbs as a whole sheet as has been suggested,[67,68] it will have a significantly slower diffusion coefficient than single unassociated thiols. Hence, the chance of the sheet diffusing away from the electrode before is can readsorb is much lower than and unassociated thiols therefore more readsorption occurs, as observed with the smoother surfaces.

Further evidence for hydrophobic forces between alkyl chains making the SAM robust comes from the position and peak shape for the reductive desorption of the SAM on the different surfaces. The potential required to remove the SAM becomes progressively more negative with the smoother surfaces (Figure 6). The one anomaly to this trend is the Ti−Au−glass surface where despite being the third roughest film the potential required to desorb the SAM is more negative than all the others. This surface also produced anomalous results for enzyme electrodes fabricated on different gold surfaces.[69] The more negative potentials on the smoother surfaces implies that the SAMs are more stable.[55] This greater stability with respect to reductive desorption is due to increased cohesive interactions and a decrease in permeability to ions and solvent with larger domains of alkanethiols on the surface. Larger domains of alkanethiols are present on the smoother surfaces because of how the monolayers form. The formation of monolayers commences through homogeneous nucleation and aggregation of absorbates on atomically smooth terraces to form domains. Several domains can form on a terrace, but over time smaller domains on a terrace may merge to form larger domains. As the size of the domain is restricted by the size of the terrace, surfaces with more discontinuities between terraces will have smaller terraces and hence smaller domains.

(67) Yang, D.-F.; Wilde, C. P.; Morin, M. *Langmuir* **1997**, *13*, 243.

(68) Yang, D.-F.; Wilde, C. P.; Morin, M. *Langmuir* **1996**, *12*, 6570.

(69) Losic, D.; Gooding, J. J.; Shapter, J. G.; Hibbert, D. B.; Short, K. *Electroanalysis*, submitted.

Printed SAMs. The horizontally printed SAMs exhibited the same trend as the solution-assembled SAMs: the smoother the substrate, the fewer the defects in the resultant SAM (Table 3). The printed SAMs however were much more permeable than SAMs formed in solution. This higher permeability indicates that the horizontally printed SAMs contain significantly more defects than the solution-formed SAMs. The poorer passivating ability of the printed SAMs relative to solution-assembled SAMs is powerfully illustrated in Figure 4 where CVs of ferricyanide on HDT-modified flat gold are exponential-shaped if the SAM is solution-assembled but peak-shaped if the SAM is printed. The greater number of defects in the printed SAMs is not only emphasized in the peak-shaped CV when investigating heterogeneous electron transfer, but also the high values of k_{app} and the large fraction of the SAM surface covered with pinholes. The inferior integrity of the printed SAMs, relative to solution assembled SAMs, is also reflected in the robustness of the printed SAMs (Figure 5) where, with repeated cycling to measure the number of pinholes, even the best printed SAM shows a far more dramatic increase in the number of pinholes on the second cycle. The number of defects with further cycling were too great to measure with this technique.

The electrochemical assessment of the horizontally printed SAMs relative to the solution-formed SAMs is in contrast to the observations of Larsen et al.,[34] who reported, using STM imaging and wetting studies, that indistinguishable quality between printed and solution SAMs can be achieved provided the concentration of alkanethiol in the ink was 10 mM or greater. The STM images performed in this study also showed no difference between the printed and solution-formed SAMs although a lack of a high impedance unit on the STM used prevented atomic resolution imaging being performed. The difference between our observations and those of Larsens et al.[34] may reflect the difference in the assessment methods and assessment environments. The STM imaging provides a qualitative assessment of the SAM based on the presence of a similar number of the same type of features and structural order on a nanometer scale. In contrast, the electrochemical assessment quantitatively measures average behavior on a macroscopic scale in an aqueous environment. In the case of developing electrochemical biosensors, this quantitative assessment directly relates to the desired function of the SAM and is more valuable for our purposes.

Reductive desorption studies show the significant differences between solution-formed and printed SAMs with regards to electrochemical passivation of the electrodes may be due to the amount of alkanethiol adsorbed. In the case of the smoother surfaces the coverage data in Tables 2 and 3 shows a slight, but not statistically significant, trend to less thiol adsorbed with the printed SAMs. In the case of the rougher gold surfaces (bulk gold and mica gold), much less thiol is adsorbed with the printing. The lesser amount of thiol adsorbed suggests that when printing, the thiol is less able to adsorb onto the low regions between grains than when the SAM is formed from solution. This hypothesis is supported by the much lower amount of thiol that adsorbs onto the very rough gold−mica substrate when the SAM is printed. With the substrates with considerable microscopic roughness the PDMS will not be able to conform to these topographical changes and hence there will be regions of the surface that do not contact the stamp, and therefore no thiol is transferred to the gold. On the smoother gold surfaces much more of the gold surface contacts the stamp, and hence a greater amount of alkanethiol adsorbs. As assembly from solution does not rely on the contacting of two surfaces, the surface roughness does not have the same influence on the amount of thiol adsorbed.

The rapid preparation and controlled positioning of the SAM afforded by microcontact printing however is highly advantageous, and therefore we investigated whether the integrity of the printed SAMs could be improved. The rolling method of depositing the SAM, where the thiol inked PDMS stamp is rolled from one end to the other until the entire stamp was in contact with the substrate, provides a more continuous SAM with less pinholes than printing (see Table 3 and Figure 4). The rolled SAMs, however, are still slightly inferior to the solution-formed SAMs. The greater integrity of the SAMs formed via the rolling method also seems to be related to the amount of alkanethiol adsorbed. The reductive desorption studies in Table 3 show that more thiol is adsorbed if the SAMs are printed with the rolling method rather than the horizontal approach. The greater amount of thiol adsorbed is presumably because, as the stamp is being rolled, thiol is being squeezed across the surface, and some of the crevices are being exposed to the thiol.

Conclusions

The surface topography of six different gold substrates has shown that, in the case of both microcontact printed SAMs and SAMs formed from solution, the smoother the surface, the higher the integrity of the SAMs as determined using electrochemical methods. Within a given method of preparing a SAM the important factor in fabricating a defect-free SAM is not the amount of alkanethiol adsorbed but the number of grain boundaries in the surface. Increasing roughness caused by the presence of imperfections leads to SAMs with poor uniformity as well as far less stability to electrochemical cycling. The SAMs formed from solution were more robust and provided a superior passivation layer over the gold electrode surface with fewer defects than the printed SAMs where the inked stamp was horizontally contacted with the substrate. The poorer quality of the printed SAMs, at least on the rougher surfaces, appears to be a result of less alkanethiol being adsorbed on to the gold surface than when the SAMs were assembled from solution. Rolling the stamp across the surface rather than horizontally contacting the surface resulted in a greater amount of thiol being adsorbed and superior SAMs being prepared. The SAMs printed with the rolling method were only marginally inferior to the solution formed SAMs but took only a few minutes rather than 24 h to prepare.

Acknowledgment. Funding from the Australian Research Council and Australian Institute of Nuclear Science and Engineering is gratefully acknowledged. Ken Short from ANSTO has provided invaluable AFM expertise and many helpful suggestions during these experiments. We thank Professor Brynn Hibbert for useful comments on this manuscript.

LA001462T